

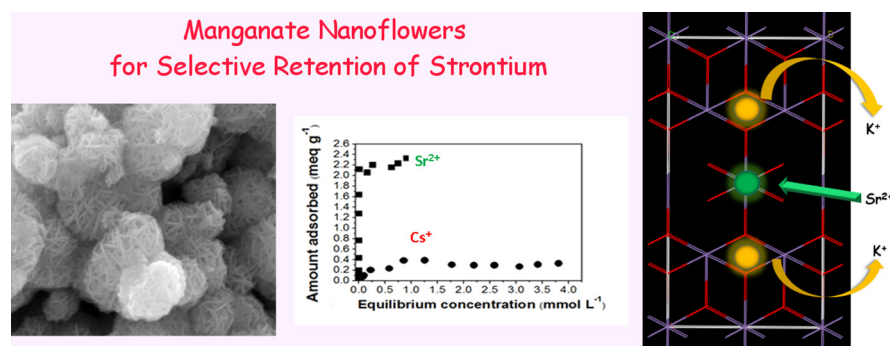


Microwave-assisted hydrothermal synthesis of manganate nanoflowers for selective retention of strontium

Delhia Alby, Fabrice Salles, Amine Geneste, Bénédicte Prélot, Jerzy Zajac, Clarence Charnay*

Institut Charles Gerhardt de Montpellier, CNRS UMR 5253, Univ Montpellier, CNRS, ENSCM, Place Eugène Bataillon, 34095, Montpellier cedex 5, France

GRAPHICAL ABSTRACT



ARTICLE INFO

Keywords:

Manganate nanoflowers
Hydrothermal synthesis
Microwave-assisted synthesis
Adsorption selectivity
Strontium
Cesium
Multicomponent aqueous solutions
Radioactive remediation

ABSTRACT

An alternative microwave-assisted hydrothermal route for the preparation of manganate nanoflowers under basic conditions has been proposed in view of potential uses in selective retention of strontium from multi-component aqueous streams. Based on the combination of such characterization techniques as Scanning and Transmission Electronic Microscopy, X-ray photoelectron spectroscopy, and X-ray Diffraction, as well as taking advantage of the computer-aided structure simulation, homogeneous nanoflower morphology possessing a layered structure and K⁺ compensating cations was evidenced as corresponding to the KMn₄O₈ chemical formula. The nanoflower sample was subsequently tested for the selective adsorption of strontium and cesium by measuring the individual adsorption isotherms from single-solute and multicomponent aqueous solutions. The material appeared selective towards strontium against cesium even in multicomponent solutions provided that the concentration of calcium remained low. This difference in the retention selectivity was rationalized based on the Density Functional Theory (DFT) calculations of the energy of adsorption and direct calorimetry measurements of the enthalpy of displacement for the individual cations.

1. Introduction

Two dimensional metal oxides have attracted increasing research interest due to their multiple functionalities, such as electronic

behavior, optical and charge transfer properties, surface reactivity, large specific surface area, mechanical flexibility [1–3]. Various stacking nanostructures were elaborated with the 2D nanosheets in order to design advanced materials with tailored properties [4].

* Corresponding author at: Institut Charles Gerhardt de Montpellier, Université de Montpellier, CC1701, Place Eugène Bataillon, 34095, Montpellier cedex 5, France.

E-mail address: clarence.charnay@umontpellier.fr (C. Charnay).

<https://doi.org/10.1016/j.jhazmat.2019.01.064>

Received 28 August 2018; Received in revised form 15 January 2019; Accepted 18 January 2019

Available online 22 January 2019

0304-3894/ © 2019 Elsevier B.V. All rights reserved.

Therefore, the development of single or multilayer materials has gained a broad attention and has demonstrated its value in a wide range of applications like in catalysis and electrocatalysis [5–10], nanoelectronics [11,12], fuel cells or energy storage devices [13], gas sensors [14] and biosensors, photovoltaic devices [15], biomedical research [1], gas barrier layers, and many others [16]. Layered materials are also known to be efficient adsorbents for the removal of radioactive and heavy metal cations [17–21]. Indeed, the interlayer space of a lamellar structure can fit to the dimension of the inserted ions or molecules through a swelling/shrinking process as the interaction between the layers is weak and easily breakable. These properties have been largely exploited during the exfoliation of inorganic nanosheets or intercalation of molecules and ions, thus resulting in the modification of numerous material properties (flexibility, layer rigidity, reactivity, porosity, hydrophilic-lipophilic balance, etc.) [17,22–25]. As a typical example of potential uses, the swelling clays were tested for the selective removal of heavy metals [26].

Nevertheless, the development of new ion-exchange materials remains an important goal for the purification of the radioactive aqueous effluents produced from the activities of the nuclear power stations, research centers or military sites, or arising from nuclear accidents or decontamination processes [18,27]. Such inorganic materials as zeolites and clays have been fully investigated as an alternative to organic resins [28,29]. More recently, layered titanates or manganates have been proposed as plausible candidates for remediation purposes on account of their high sorption capacity and selectivity towards some monovalent or divalent cations [30,31].

Titanate and manganate nanomaterials have been largely studied over the years regarding their different dimensional structures (1D, 2D or 3D) [25,32] in decontamination uses [33] and green chemistry [34]. Birnessite-like phases, the most investigated synthetic manganate nanostructures, are related to natural phyllosilicates which exhibit a basal spacing of 7 Å for one layer of structured water in the case of the birnessite and 10 Å for two layers of water in the case of the busierite structure. This layered structure presents edge sharing MnO_6 octahedra with a net negative layer charge due to the intra-framework substitution of Mn^{3+} for Mn^{4+} , balanced by various interlayer cations such as Na^+ , Ca^{2+} or K^+ [35]. This material is especially interesting as ion exchanger, since it can fix cations very strongly [27,33,36,37]. Several synthesis pathways were investigated to optimize its structure and properties useful for many different applications [7]. Since then, the efforts have focused on various nanostructures that this material can produce (i.e., nanotubes, nanobelts, nanoflowers...) [6,13,25]. It was shown that their optical and electronic properties were dependent on the shape, size, and crystallographic structure [9]. Moreover, these manganese oxides exhibited notable surface charge due to their redox properties (versatility of the manganese oxidation number) leading to noticeable cation-exchange properties and thus a high reactivity in sorption phenomena [35]. It was reported that the cation exchange in these materials occurred within the interlayer space being accompanied by a layer swelling mechanism [33,38,39]. However, the manganate nanoflowers or manganate nanospheres achieved by a hydrothermal synthesis route in an acid medium were demonstrated to exhibit a poor performance for Sr^{2+} retention [40].

In the present study, a microwave assisted hydrothermal synthesis in basic conditions was proposed to obtain homogenous manganate nanoflowers. In regards with cesium and strontium isotopes representing the predominant radionuclides released into the environment after a nuclear accident, the sorption performances of such nanoflowers were tested in different aqueous media so as to monitor various competitive effects occurring during the adsorption process carried out under conditions close to real uses. The combination between the results of Density Functional Theory (DFT) calculations and isothermal titration calorimetry measurements contributed to shed light on the ion-exchange mechanism within manganate nanoflowers.

Table 1

Composition of two mineral waters used to prepare cesium and strontium solutions for the purpose of retention tests.

Ions	Mineral water rich in Ca^{2+} (mmol L^{-1}) pH = 7.60	Mineral water rich in Na^+ (mmol L^{-1}) pH = 5.85
Ca^{2+}	1.57	0.06
Mg^{2+}	0.42	0.04
Na^+	0.06	0.14
K^+	0.01	0.01
HCO_3^-	2.84	0.10
SO_4^{2-}	0.53	0.02
NO_3^-	0.03	0.05
Cl^-	–	0.08

2. Experimental

2.1. Materials

Potassium permanganate was obtained from Prolabo, hexadecylamine (> 94%) from Merck Millipore, whereas cesium nitrate (99%), strontium nitrate (98%) and calcium nitrate tetrahydrate (99%) were Sigma-Aldrich products. Ultrapure water was obtained with a Purelab purification system ($18 \mu\text{S cm}^{-1}$). Regarding the adsorption isotherms, the different compositions of mineral water used as mean solvents are reported in Table 1.

2.2. Material synthesis and characterizations

Manganate nanoflowers were obtained through a hydrothermal synthesis under microwave radiation in a Teflon autoclave with a StartSynth® oven from Milestone Company. The magnetron delivered a puissance up to 1200 W (2400 Hz) and the temperature was controlled by an optical fiber system.

The nanoflower synthesis was adapted from a conventional hydrothermal synthesis of manganate nanotubes in a classical oven [5]. Different parameters were investigated, including the temperature and duration of the hydrothermal treatment under microwave radiation. The duration of the first step corresponding to the addition of the amine template into the manganate solution was also an adjustable parameter (not investigated here). In a typical synthesis, 50 mL of a solution obtained by dissolving potassium permanganate (4.2 g; 0.026 mol) with KOH (9.31 g; 0.166 mol) were stirred during 15 min, prior to the addition of hexadecylamine (1.15 g; 0.047 mol). The suspension was then placed in a high-pressure vessel from Milestone® composed of a PTFE vessel and a PEEK shield and heated at 463 K for 2 h under microwave radiation. The obtained material was washed with ultrapure water and dried at 343 K.

The wide-angle X-ray diffraction (XRD) patterns were obtained at ambient temperature with a Philips X'pert 0-0 diffractometer equipped with a X'Celerator detector by using Cu K α radiation ($\lambda = 0.15418 \text{ nm}$) and a fixed power source (45 kV and 30 mA). The small-angle diffraction patterns (2θ from 1.5° to 10°) were recorded with a $1/16$ slit.

XRD at different temperatures from 293 K to 873 K were recorded under vacuum (0.1 Pa) with an Empyrean X-ray diffractometer with the Cu K α radiation and a 0.016° step. Analysis lasted 1 h for each temperature level increasing progressively up to 873 K and then the temperature returned to 293 K.

Scanning Electron Microscope (SEM) observations were realized on a microscope FEI Quanta 200 FEG with high-resolution field emission to determine the shape and the morphology of the synthesized particles. Moreover, the morphology of the nanostructures was visualized with Transmission Electron Microscopy (TEM). The analyses were realized on a JEOL 1200EX2 with an acceleration tension of 100 kV and the images were captured by a SIS Olympus camera (Quemesa model) with a CDD captor of 11 Mpixels.

The metal oxidation states and the surface composition of the samples were determined by X-ray photoelectron spectroscopy (XPS) using an ESCALAB 250 spectrophotometer from Thermo Electron. The excitation source was monochromatic (Al K α (1486.6 eV)) and the analyzed surface corresponded to a 400 μm diameter. The photoelectron spectra were calibrated in bond energy in agreement with the energy of the component C–C from carbon C1s at 284.8 eV. The metal content, manganese or potassium, in weight percent was corroborated by Inductively Coupled Plasma-Optical Emission Spectrometry (ICP-OES) with a Perkin Elmer Optima 7000 DV. This method was also used to measure the amount adsorbed of strontium. The material was first dissolved in acid media (nitric and perchloric acids) and the measurement was realized by axial view for manganese and radial view for strontium.

2.3. Adsorption

In order to evaluate the retention performance (capacity and selectivity) of the manganate nanomaterials towards cesium and strontium ions, their adsorbed amount Γ_{ads} and the adsorption isotherms were determined according to the depletion method with the following procedure. A solid sample (0.020 g) was first placed into a Nalgene[™] reactor and a 20 mL solution of cesium nitrate (from 0.05 mmol L⁻¹ to 4 mmol L⁻¹) and/or strontium nitrate (from 0.03 mmol L⁻¹ to 2.5 mmol L⁻¹) was added. To reach the adsorption equilibrium, the tubes were stirred on a rotary shaker overnight at 298 K. To separate the solid phase from the liquid supernatant, the tubes were centrifuged at 11,000 rpm for 10 min. After filtration (porosity of 0.22 μm), the supernatant was analyzed by Ionic Chromatography (IC). The cationic composition was thus determined with a Shimadzu device composed by a Shim-pack IC-C1 column and a CDD-6 A conductivity detector at 313 K. The volume of injection was of 45 μL and the flow rate of 1.5 mL min⁻¹. The mobile phase used to measure the cation content was composed of nitric acid (5 mmol L⁻¹) for cesium analysis and a mixture tartaric acid (4 mmol L⁻¹) and ethylenediamine (1.4 mmol L⁻¹) for strontium and calcium analysis.

The enthalpy changes accompanying adsorption were measured in a differential titration nanocalorimeter in a heat flow mode and installed in a TAM III thermostat working at a constant temperature kept at 298 K within ± 0.0001 . The operating procedures and data processing were detailed previously [41]. A 4 mg solid sample was introduced into the calorimeter cell containing 0.8 mL of ultrapure water and maintained under constant stirring for 2 h to attain the thermal equilibrium (the reference cell was only filled with water). A syringe system was used to perform 10 s injections of 10 μL of the appropriate solution (cesium or strontium nitrate). The thermal peaks were recorded after an equilibrium of 45 min between two injections and the area under each peak was determined to calculate the corresponding enthalpy change. A similar procedure was employed to evaluate the effect of dilution [41]. Each calorimetric run was repeated 3 times.

2.4. Computational part

2.4.1. Structure simulation and parameters for manganese oxide

The computational effort was made to determine a correct model of

the structure for manganese oxide saturated with K⁺ as interlayer cations. The initial atomic coordinates of the framework were taken from the literature after comparison with different birnessite structures. The structure built from Post and Veblen was used [42]. Then, the unit cell parameters were fixed based on the XRD data obtained in this work as a function of the nature of the interlayer cation and using a C2/C symmetry. Finally, a plausible crystallographic structure was proposed with the imposed symmetry.

Theoretical diffractograms were thus generated with Reflex software using the simulated structures and further comparison with the experimental data allowed the nature of the synthesized solids to be confirmed.

2.4.2. Determination of accessible surface area and pore volume

Following Düren et al. [43], both the accessible surface area and the pore volume of the simulated structure models were calculated. The surface was thus calculated using the center of a nitrogen probe molecule rolling across the surface. In this case, the diameter of the nitrogen probe molecule was fixed at 368.1 pm, while the Universal Force Field (UFF) was used for the framework atoms [44].

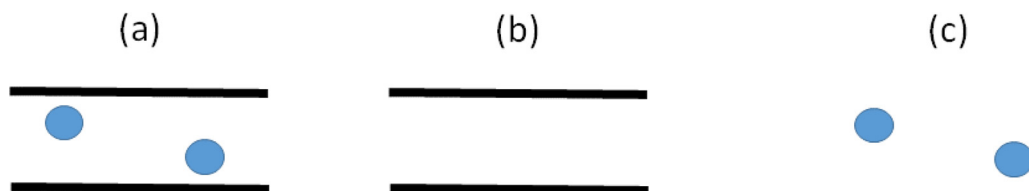
2.4.3. Exchange energy determination

In order to estimate the energy required to replace the interlayer cation, Density Functional Theory (DFT) calculations were performed on the structures containing interlayer cations. For this purpose, the previous structures validated by comparison with the experimental XRD patterns were considered as the starting point. The so-obtained models were therefore geometry optimized based on DFT calculations assuming fixed unit cell parameters. In complement, calculations were also performed on both the cations (K⁺, Ca²⁺, Sr²⁺, Cs⁺) alone and the corresponding structures without interlayer cations so as to determine the adsorption energy using the following equation: $E_{\text{ads}} = E_{\text{Cox}} - E_{\text{Ox}} - E_{\text{C}}$ where E_{Cox} , E_{Ox} and E_{C} correspond to the energy of the oxide structure with C⁺ cations, the one without C⁺ cations and the intrinsic energy of C⁺. The base of this calculation is summarized in the Scheme 1.

To ensure consistency in the comparison of data, the calculations were done on the double cell (i.e., according to the b axis if c corresponds to the axis of the stacking). These DFT calculations were performed using a DFT approach with a double numerical radial function basis set (DMol³ software package) as well as the PW91 GGA density functional containing polarization functions on hydrogen atoms (DNP).

3. Results and discussion

Manganate nanoflowers were initially reported by direct electro-deposition of manganese oxide on a substrate consisting of a film of carbon nanotubes [6]. A synthesis route at low temperature was also described by mixing potassium permanganate and formamide for 8 h [7]. Microwave-assisted synthesis methods have been used for several years to synthesize various porous adsorbents because the microwave energy can lead to much higher heating rates, thereby improving their preparation and decreasing significantly the synthesis time from days to hours [45,46]. Manganate nanoflowers were achieved in this way by hydrothermal method in acid medium at 373 K performed for 25 min



Scheme 1. Evaluation of the adsorption energy for the cation (in blue) between manganate layers (in black). This energy obtained from DFT calculation corresponds to the difference between the energy of (a) and the sum of (b) and (c). (For interpretation of the references to colour in this Scheme legend, the reader is referred to the web version of this article).

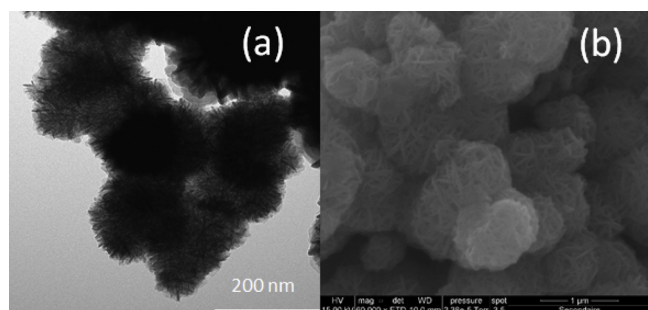


Fig. 1. Manganate nanoflowers observed by (a) TEM and (b) SEM.

under microwave irradiation [47]. An alternative procedure with a microwave-assisted hydrothermal treatment in basic conditions is proposed in the present work.

The morphology of the structure was observed by Scanning Electron Microscope (SEM) and Transmission Electron Microscopy (TEM) where distinct nanoflower structures appeared well formed and homogeneous (Fig. 1).

Fig. 2 displays XRD diagrams which give information on the interlayer distance of the synthesized lamellar nanostructure. The interlayer distance is equal to 760 pm using the first diffraction peak assigned to the (001) crystal plane (coherent with the C2/m symmetry considered for the structure refinement). Furthermore, the chemical composition (the amount of nitrogen and carbon) was determined by elemental analysis. The potassium and manganese contents were estimated by ICP-OES analysis at 3.2 wt% and 12.0 wt% respectively, whereas the different oxidation numbers of manganese and the proportion were assessed by XPS. Elemental analysis confirmed the absence of the amine template in the final material, since no nitrogen was detected whereas only carbon traces (0.60 wt%) were measured. This evidences that the amine has been totally removed throughout the washing step. Moreover, the material is mainly composed of Mn (IV) with some traces of Mn (III), as inferred from the XPS analysis (Fig. S1 in Supporting Information). The chemical formula corresponds to KMn_4O_8 . Taking this formula for simulation of the nanostructure, it was possible to compare the simulated diffraction patterns with the experimental ones. As reported in Fig. 2a, a very good agreement was found, thus indicating that the theoretically generated structure coincided with that of the synthesized solid. Moreover, the concordance between the simulated and experimental X-ray diffraction patterns confirms that no other crystalline phase containing manganese is present in the sample. The so-obtained material therefore presents a monoclinic structure (C2/m) with $a = 514.9$ pm, $b = 568.6$ pm, $c = 731.0$ pm and $\beta = 100.76^\circ$. Using this structure, such textural properties as specific surface area and pore volume could be estimated theoretically. Such data could not be obtained experimentally from the results of gas nitrogen adsorption at

Table 2

Unit cell parameter, c , hydrated radius for the cations [51], specific surface area, SSA, and pore volume, PV, as obtained by molecular simulations for XMn_4O_8 where $X = \text{K}^+$, Cs^+ and Sr^{2+} .

	c (Å)	Hydrated radius (Å)	SSA N_2 ($\text{m}^2 \text{g}^{-1}$)	PV ($\text{cm}^3 \text{g}^{-1}$)
K^+	7.31	3.31	1120	0.16
Cs^+	7.54	3.29	1118	0.18
Sr^{2+}	6.92	4.12	892	0.15

77 K since a thermal pre-treatment under vacuum is required before the measurement of the adsorption isotherm. Such a step leads to the closure of the interlayer space of the solid due to the dehydration. However, the lamellar materials keep their structure as already observed in the case of the swelling clays [48]. Moreover, these conclusions are well supported by Fig. S2 in Supporting Information. When the temperature is increased to 373 K under vacuum, a shift of the (001) peak to the wide angles is observed on X-ray diffraction diagram in agreement with the collapse of the interlayer space. In consequence, the molecular simulation was the only way to evaluate these parameters (see Table 2). It is important to note however that the compound is stable up to 873 K, as evidenced by XRD in Fig. 2b. This thermal stability is of high importance in view of potential uses of the material in the high level waste disposal or thermal catalytic degradation in which the temperature can reach 400–500 K [14,49,50]. It follows that the structure slightly evolves upon ion exchange between K^+ and Cs^+ , which leads to comparable textural properties. The range of specific surface area is in good agreement with the values generally obtained in the case of swelling clays such as montmorillonites: their specific surface areas can vary from 300 to 1200 $\text{m}^2 \text{g}^{-1}$ as a function of the nature of the interlayer cation [48]. In contrast, the solid saturated with Sr^{2+} undergoes shrinkage of the structure probably due to the higher cation charge compared to those of alkali cations.

3.1. Adsorption performance of manganate nanoflowers

Adsorption isotherms for strontium and cesium cations were measured to determine the adsorption capacity and affinity of the solid material towards a given cation by using ultrapure water and two types of mineral water (their compositions are reported in Table 1) to prepare aqueous solutions of strontium and cesium. The results obtained at 298 K are given in Fig. 3. Regarding the adsorption of Sr^{2+} , the adsorption isotherms represent high-affinity curves with a quasi-vertical initial portion and a saturation plateau at higher equilibrium concentrations. When this bivalent cation is adsorbed from aqueous solutions in ultrapure water, the initial steep portion of the isotherm can extend up to an amount adsorbed of 1.1 mmol g^{-1} , whereas the maximum adsorption capacity is about 1.2 mmol g^{-1} (2.4 meq g^{-1}). In this case, the distribution coefficient (K_d in mL g^{-1}) can be evaluated in

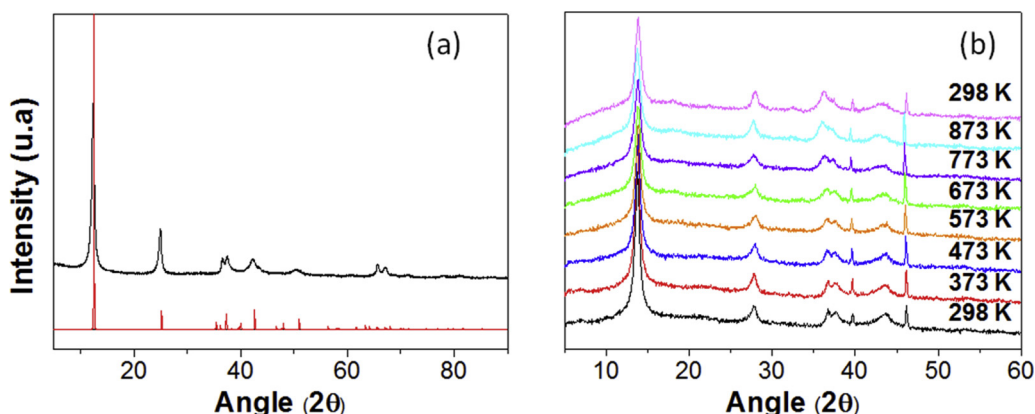


Fig. 2. X-Ray diffraction patterns for manganate nanoflowers (a) at ambient temperature : experimental (black line) and simulated data (red line), (b) under vacuum: at 298 K (black), 373 K (red), 473 K (blue), 573 K (orange), 673 K (green), 773 K (purple), 873 K (cyan), back to 298 K (pink) (For interpretation of the references to colour in this figure legend, the reader is referred to the web version of this article).

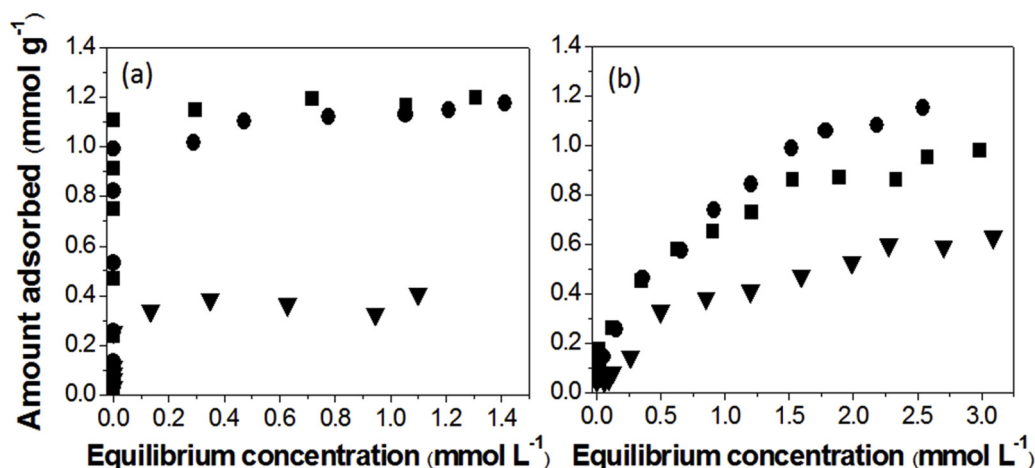
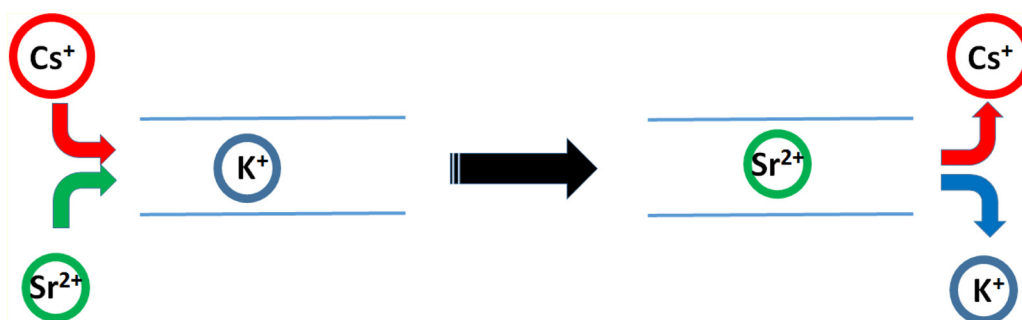


Fig. 3. Isotherms of (a) strontium and (b) cesium adsorption onto manganate nanoflowers at 298 K from aqueous solutions in ultrapure water (squares), mineral water rich in Na^+ (circles), and mineral water rich in Ca^{2+} (triangles).



Scheme 2. Schematic diagram for the preferential adsorption of Sr^{2+} in manganates.

Henry's law region [18]. The value of $\text{Log}(K_d)$ estimated in this manner is about 6 which indicates that almost all strontium cations available in the solution have been retained by the solid surface, thereby replacing the potassium counter-ions initially present in the interlayer space, as described in Scheme 2. Moreover, the exchange mechanism thus described is well supported by the exchange ratio between the desorbed K^+ and adsorbed Sr^{2+} which is close to 2 as displayed in Fig. S3 in Supporting Information.

According to the layered structure of manganate nanoflowers, the interlayer space of their lamellar structure can adjust to fit to the large dimension of the inserted Sr^{2+} ions (hydrated radius of 0.412 nm) [51] through a swelling/shrinking process. The above-mentioned performance parameters of the manganate nanoflowers can be compared with similar parameters reported for other materials in the literature on the subject. Much better sorption performance is unambiguously notified for the present sample when the comparison is made with hydroxyapatite, usually regarded as the reference with a retention capacity being of 0.4 mmol g^{-1} [52], or even when compared with bentonite (0.6 mmol g^{-1}) [53]. Note that the same maximum retention capacity has been obtained with a zeolite A sample [28].

When the adsorption is performed under competitive conditions (i.e., mineral water rich either in Na^+ or in Ca^{2+}), strontium cations may enter into competition with some other ions present in the solution. In aqueous solutions prepared from mineral water rich in sodium, only a very small decrease down to 1.1 mmol g^{-1} in the retention capacity is observed. On the contrary, with a mineral water rich in Ca^{2+} , the amount adsorbed is markedly reduced and it levels off at about 0.4 mmol g^{-1} . This ultimately points towards a strong competition from the cations accompanying strontium in solutions with different compositions. Logically, calcium should be the main competitor, as it is present in large quantities in the systems studied. Its depressing impact

on the strontium adsorption has been reported previously [54–56].

To better probe the competition between strontium and calcium in the system studied and thus to shed more light on the retention selectivity of the present material, supplementary measurements of individual calcium adsorption have been done in single-solute and bi-solute (in competition with Sr^{2+}) systems. The results are reported in Fig. 4 and compared with the corresponding adsorption isotherms for strontium. When each cation is adsorbed from single-solute solutions (c.f., Fig. 4a), the two adsorption curves are very similar. They appear as having almost the same affinity towards the manganate nanoflower structure. Thus, it is not surprising that they will compete against each other when present together in aqueous solutions. When the adsorption process is studied in aqueous solutions containing both competitors in equimolar 1:1 proportions, their mutual competition results in a quite similar depression of the amount adsorbed down to about 0.5 mmol g^{-1} , especially at low equilibrium concentrations, as can be seen in Fig. 4b.

As far as the adsorption of cesium in similar systems is concerned, the adsorption isotherms represent curves with a low affinity in the initial concentration range (c.f., Fig. 3b). In view of potential uses in the selective removal of strontium and cesium from nuclear waste water, an important conclusion drawn from the comparison of the adsorption curves in this early stage of individual adsorption in single-solute systems is that the manganate nanoflowers synthesized in the present work are highly selective for strontium against cesium. It is worth noting that this selectivity is still valid when both solutes are adsorbed from aqueous solutions in mineral water rich in Na^+ (c.f., Fig. 3b). In the range of higher equilibrium concentrations, the retention capacity of the solid sample appears to strongly depend on the mutual concentrations of cations in the equilibrium solutions. For example, the maximum amount of cesium adsorbed onto manganate nanoflowers within the

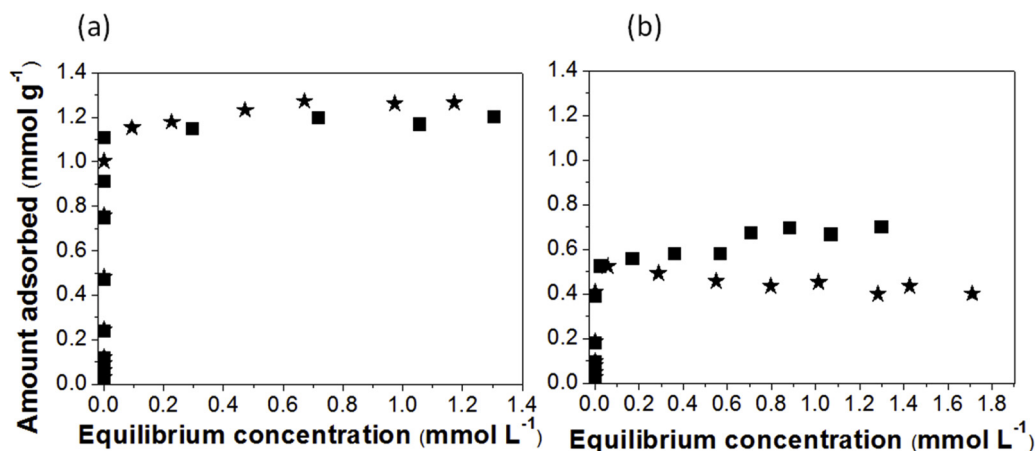


Fig. 4. Isotherms of strontium (squares) and calcium (stars) adsorption onto manganese nanoflowers from (a) single-solute and (b) bi-solute solutions at 298 K.

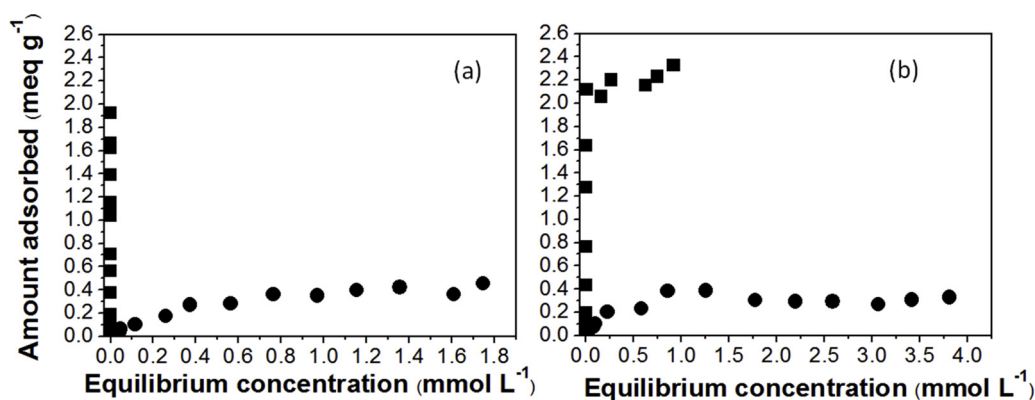


Fig. 5. Individual isotherms for cesium (circles) and strontium (squares) adsorption onto manganese nanoflowers at 298 K from bi-solute aqueous solutions. The ratio between the initial concentrations of cesium and strontium in the stock solution was as follows: (a) 2:1 mmol L⁻¹ and (b) 4:2 mmol L⁻¹.

Table 3

Adsorption energy at saturation for different cations onto manganese nanoflowers as determined by the DFT-based calculation, together with the corresponding enthalpy of cation hydration in aqueous solution taken from Ref. [57].

Cation	$\Delta_{\text{ads}}H$ (kJ mol ⁻¹)	$\Delta_{\text{hyd}}H$ (kJ mol ⁻¹) [57]
Sr	-1096	-1470
Ca	-1097	-1600
Cs	-196	-280
K	-252	-330

concentration range studied in the present work reaches about 1.0 mmol g⁻¹ in ultrapure water and 1.1 mmol g⁻¹ in mineral water rich in Na⁺. This slight upward tendency in the retention capacity can likely be ascribed to the positive effect of the increased ionic strength in the presence of numerous ionic species in the aqueous phase. Anyhow, none of those ions can greatly affect the individual affinity of strontium or cesium species for the manganese structure. On the contrary, the presence of Ca²⁺ in great quantities has a detrimental effect also on the retention of cesium. The effect is pronounced at very low equilibrium concentrations where the individual adsorption of this species is strongly decreased (Fig. 3b). When the equilibrium concentration of Cs⁺ increases, its adsorption quantity becomes continuously greater up to about 0.6 mmol g⁻¹ at the end of the concentration range studied here.

In further adsorption experiments, strontium and cesium cations have been put in direct competition with each other within the bi-solute aqueous solutions prepared using ultrapure water. The corresponding ratios between the initial concentrations of cesium and strontium in the

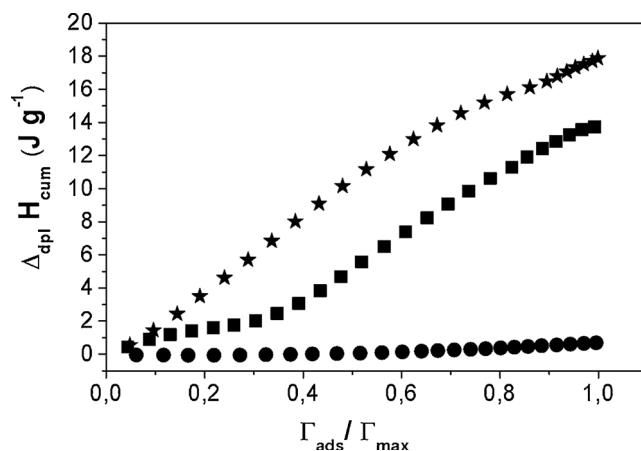


Fig. 6. Evolution of the cumulative enthalpy of displacement accompanying adsorption of cesium (circles), strontium (squares), and calcium (stars) onto manganese nanoflowers at 298 K from single-solute aqueous solutions as a function of the surface coverage by the adsorbing cation. The surface coverage $\Gamma_{\text{ads}}/\Gamma_{\text{max}}$ is calculated from the adsorbed amount (Γ_{ads}) normalized with the maximum adsorbed amount (Γ_{max}).

stock solution were 2:1 mmol L⁻¹ (for the overall ionic strength being comparable to that obtained in the previous experiments) and 4:2 mmol L⁻¹ (for the specific concentrations being comparable with those tested in the previous experiments). The individual adsorption isotherms inferred from these experiments have been plotted in Fig. 5a and b. The comparison between the shapes of the adsorption curves in the very

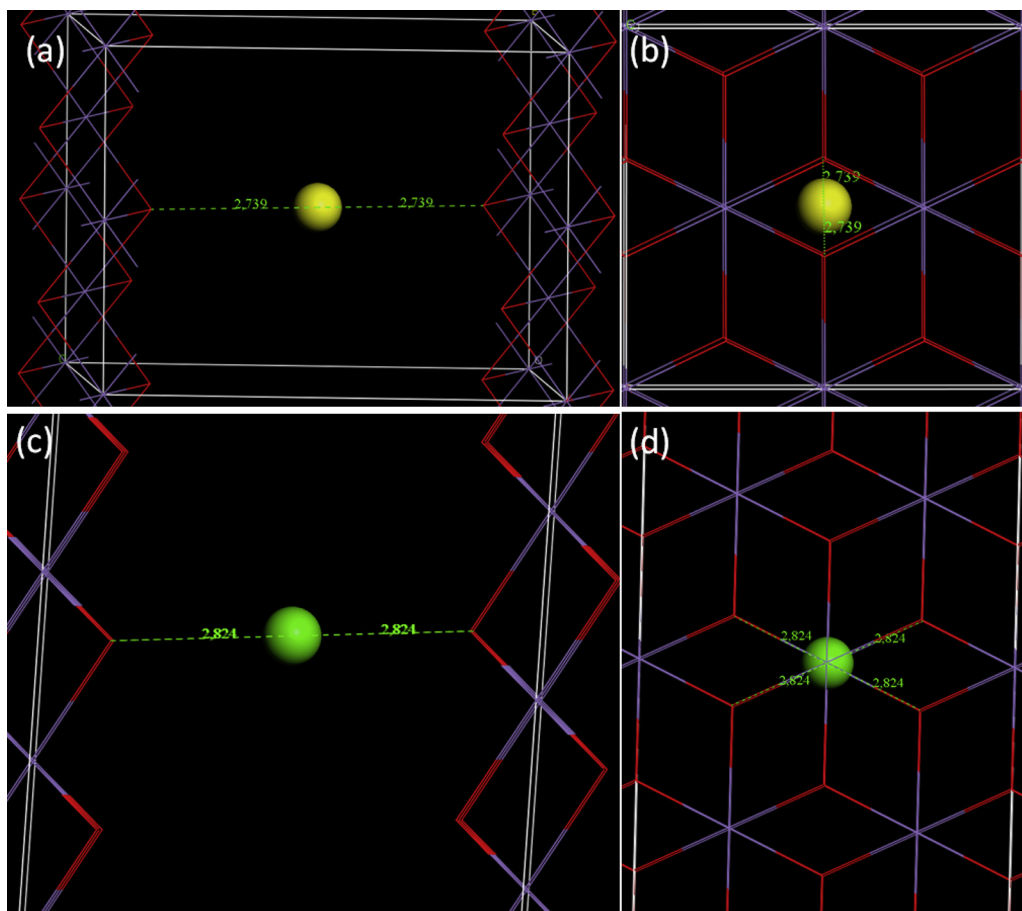


Fig. 7. Snapshots showing the positions of the compensating cations inside the manganate layers for Cs^+ (yellow) (a) and (b) and Sr^{2+} (green) (c) and (d). Violet and red elements represent V and O atoms, respectively. The snapshots (a) and (c) correspond to a projection according to the xz plan, while (b) and (d) correspond to a projection according to the xy plan (For interpretation of the references to colour in this figure legend, the reader is referred to the web version of this article).

beginning of the concentration range reinforces the hypothesis formulated previously that only strontium is retained by manganate nanoflowers in this initial adsorption range. In the absence of other ionic species in the aqueous phase, cesium cannot compete effectively with strontium at very low concentrations. When the overall concentration of the equilibrium solution increases (at the same initial molar proportions between the two solutes), cesium can be retained by the material but to a much lesser extent attaining a steady value of about 0.4 meq g^{-1} in the adsorption plateau region, irrespective of the Cs:Sr concentration ratio. For higher strontium concentrations in the equilibrium bulk phase, a saturation plateau is also observed (Fig. 5b) with an adsorption quantity of 2.2 meq g^{-1} (1.1 mmol g^{-1}). This value is slightly smaller than the one measured in the single-solute systems but equal to that determined when the adsorption phenomenon has been carried out in solutions prepared using mineral water rich in sodium. This indicates again a very small effect on the strontium retention produced by competing monovalent cations, like Na^+ and Cs^+ , when present at higher concentrations.

The observed differences in the selectivity of manganate nanoflowers towards calcium, strontium, and cesium were rationalized through the DFT-based calculation of the energy of ion adsorption at saturation on the one hand and calorimetric measurements of the enthalpy of displacement accompanying ion adsorption in the single-solute systems on the other hand. The results are reported in Table 3 and in Fig. 6, respectively.

In the light of the theoretical values of adsorption energy calculated for various cations (c.f., Table 3), it is not surprising that strontium and calcium can displace very easily potassium from the interlayer space. Indeed a strong difference between divalent and monovalent cations confirms the preferential adsorption for Ca^{2+} and Sr^{2+} cations compared to that of K^+ and Cs^+ . As a similar theoretical energies of

adsorption have been obtained from DFT calculations for Ca^{2+} and Sr^{2+} , it is more difficult to propose strict differentiation between these two cations. Moreover, it is necessary to note that these energy values include also contributions due to the swelling effect, even though such an energy component should be relatively small on account of small variations of the interlayer distance upon cation exchange depending on the cation nature. In the case of cesium, its energy of adsorption being smaller than that of potassium, the effectiveness of cation exchange is very limited, especially at very low cesium concentrations where the driving force for ion-exchange is dominated mostly by the difference in the adsorption energy. A noticeable increase in the cesium concentration resulting in the increased electrochemical potential of this cation is necessary to push the cation-exchange pathway in the reverse direction. Identical energy values obtained separately for strontium and calcium argue in favor of similar adsorption behavior, as evidenced by almost the same adsorption isotherms reported in Fig. 4a. The same conclusion may be formulated when analyzing the initial portions of the individual adsorption isotherms from bi-solute solutions in Fig. 4b. Beyond this initial concentration region, there is an increase in the amount of strontium retained by the nanoflower sample at the expense of calcium adsorption. This change, even though it remains relatively small, cannot be explained only by the adsorption energy difference. Moreover, the configurations of the interlayer divalent cations inferred from molecular simulations indicate that both types of cations are located on similar sites within the layered structure, which means that the mechanism of adsorption at a microscopic scale cannot be greatly affected by cation positions (see Fig. 7). Therefore, some other contributions to the total energy and entropy balance should be taken into consideration. It is often postulated that cation exchange with the use of various inorganic oxides is a complex displacement process in which the resulting enthalpy of displacement may be

governed also by the concomitant hydration effects related to the modification of the hydration shells of adsorbing and desorbing species [58,59]. For this purpose, the values of the enthalpy of cation hydration in aqueous solutions have been collected in Table 3. The experimental enthalpies of displacement recorded for three single-solute systems are plotted as a function of surface coverage by the adsorbing cation in Fig. 6. These curves reveal great differences in the driving force for ion-exchange with potassium ions from the viewpoint of enthalpy. For cesium, the displacement process appears almost athermal. This may be easily justified by including in the difference between the energy of cesium and potassium adsorption also the difference in the hydration enthalpy (with the values given in Table 3). In the case of strontium and calcium, the overall displacement process is endothermic and thus entropy-driven. This endothermic character falls in line with the values of the enthalpy of hydration overcoming that of adsorption, as can be seen in Table 3. With the exception of the first few points, the enthalpy values measured for strontium and calcium are different. The displacement of potassium by calcium is more endothermic than that involving strontium. This likely explains why there is less calcium retained by the manganate structure in higher concentration regimes when both cations are adsorbed from equimolar bi-solute solutions (see Fig. 4b).

Finally, the ion-exchange behavior of the present layered material is in good agreement with that of some swelling clays as montmorillonites for which the effect of both the hydration of the interlayer cation and the partial charge on the ion exchange has already been proven both experimentally and theoretically [60,61].

4. Conclusion

A new synthesis route was developed to obtain homogenous manganate nanoflowers as observed by microscopy. These materials have been proved to be really efficient for the capture of strontium in aqueous media. Indeed, the maximum amount adsorbed was as high as 2.4 meq g^{-1} in ultrapure water with a value of $\text{Log}(K_d) = 6$, indicating high performances compared to those of other materials reported in the literature. The competition between calcium and strontium could be observed when a large concentration of calcium was present due to their similar interaction energies with the manganate framework. The material remained selective towards strontium against cesium even in multicomponent solutions provided that the concentration of calcium remained low, thereby allowing the manganate nanoflowers to be considered as well suited for nuclear decontamination uses.

Acknowledgments

The authors greatly acknowledge the financial support of this work by the RSNR DECLIQ project (ANR-11-RSNR-0004) in the framework of the French ANR Program 'Investments for the Future: Nuclear Safety and Radiation Protection Research'.

Appendix A. Supplementary data

Supplementary material related to this article can be found, in the online version, at doi:<https://doi.org/10.1016/j.jhazmat.2019.01.064>.

References

- [1] W. Yang, X. Zhang, Y. Xie, Advances and challenges in chemistry of two-dimensional nanosheets, *Nano Today* 11 (2016) 793–816, <https://doi.org/10.1016/j.nantod.2016.10.004>.
- [2] T. Niu, A. Li, From two-dimensional materials to heterostructures, *Prog. Surf. Sci.* 90 (2015) 21–45, <https://doi.org/10.1016/j.progsurf.2014.11.001>.
- [3] K. Kalantar-Zadeh, J.Z. Ou, T. Daeneke, A. Mitchell, T. Sasaki, M.S. Fuhrer, Two dimensional and layered transition metal oxides, *Appl. Mater. Today* 5 (2016) 73–89, <https://doi.org/10.1016/j.apmt.2016.09.012>.
- [4] M.-Y. Li, C.-H. Chen, Y. Shi, L.-J. Li, Heterostructures based on two-dimensional layered materials and their potential applications, *Mater. Today* 19 (2016) 322–335, <https://doi.org/10.1016/j.mattod.2015.11.003>.
- [5] A.J. Roberts, R.C.T. Slade, Birnessite nanotubes for electrochemical supercapacitor electrodes, *Energy Environ. Sci.* 4 (2011) 2813–2817, <https://doi.org/10.1039/c1ee01394g>.
- [6] H. Zhang, G. Cao, Z. Wang, Y. Yang, Z. Shi, Z. Gu, Growth of manganese oxide nanoflowers on vertically-aligned carbon nanotube arrays for high-rate electrochemical capacitive energy storage, *Nano Lett.* 8 (2008) 2664–2668, <https://doi.org/10.1021/nl800925j>.
- [7] J. Ni, W. Lu, L. Zhang, B. Yue, X. Shang, Y. Lv, Low-temperature synthesis of monodisperse 3D manganese oxide nanoflowers and their pseudocapacitance properties, *J. Phys. Chem. C* 113 (2009) 54–60, <https://doi.org/10.1021/jp806454r>.
- [8] M.Y. And, S. O'Brien, Synthesis of monodisperse nanocrystals of manganese oxides, *J. Am. Chem. Soc. Commun.* 125 (2003) 10180–10181, <https://doi.org/10.1021/JA0362656>.
- [9] L.-C. Zhang, Z.-H. Liu, H. Lv, X. Tang, K. Ooi, Shape-controllable synthesis and electrochemical properties of nanostructured manganese oxides, *J. Phys. Chem. C* 111 (2007) 8418–8423, <https://doi.org/10.1021/JP070982V>.
- [10] F.Y. Cheng, J. Chen, X.L. Gou, P.W. Shen, High-power alkaline Zn-MnO₂ batteries using γ -MnO₂ Nanowires/Nanotubes and electrolytic zinc powder, *Adv. Mater.* 17 (2005) 2753–2756, <https://doi.org/10.1002/adma.200500663>.
- [11] J.E. ten Elshof, Electronic band structure and electron transfer properties of two-dimensional metal oxide nanosheets and nanosheet films, *Curr. Opin. Solid State Mater. Sci.* 21 (2017) 312–322, <https://doi.org/10.1016/j.cossms.2017.08.004>.
- [12] M. Osada, T. Sasaki, Exfoliated oxide nanosheets: new solution to nanoelectronics, *J. Mater. Chem.* 19 (2009) 2503–2511, <https://doi.org/10.1039/b820160a>.
- [13] K. Chen, Y. Dong Noh, K. Li, S. Komarneni, D. Xue, Microwave-Hydrothermal crystallization of polymorphic MnO₂ for electrochemical energy storage, *J. Phys. Chem. C* 117 (2013) 10770–10779, <https://doi.org/10.1021/jp4018025>.
- [14] X. Tian, L. Yang, X. Qing, K. Yu, X. Wang, Trace level detection of hydrogen gas using birnessite-type manganese oxide, *Sensors Actuators B Chem.* 207 (2015) 34–42, <https://doi.org/10.1016/j.snb.2014.08.018>.
- [15] M.M. Furchi, A. Pospischil, F. Libisch, J. Burgdörfer, T. Mueller, Photovoltaic effect in an electrically tunable van der Waals heterojunction, *Nano Lett.* 14 (2014) 4785–4791, <https://doi.org/10.1021/nl501962c>.
- [16] L. Wang, T. Sasaki, Titanium oxide nanosheets: graphene analogues with versatile functionalities, *Chem. Rev.* 114 (2014) 9455–9486, <https://doi.org/10.1021/cr400627u>.
- [17] W.J. Roth, B. Gil, W. Makowski, B. Marszałek, P. Eliášová, Layer like porous materials with hierarchical structure, *Chem. Soc. Rev.* 45 (2016) 3400–3438, <https://doi.org/10.1039/C5CS00508F>.
- [18] D. Alby, C. Charnay, M. Heran, B. Prelot, J. Zajac, Recent developments in nanostructured inorganic materials for sorption of cesium and strontium: synthesis and shaping, sorption capacity, mechanisms, and selectivity—a review, *J. Hazard. Mater.* 344 (2018) 511–530, <https://doi.org/10.1016/j.jhazmat.2017.10.047>.
- [19] M. Galamboš, P. Suchánek, O. Roskopfová, Sorption of anthropogenic radionuclides on natural and synthetic inorganic sorbents, *J. Radioanal. Nucl. Chem.* 293 (2012) 613–633, <https://doi.org/10.1007/s10967-012-1717-y>.
- [20] B. Filipowicz, M. Pruszyński, S. Krajewski, A. Bilewicz, Adsorption of ¹³⁷Cs on titanate nanostructures, *J. Radioanal. Nucl. Chem.* 301 (2014) 889–895, <https://doi.org/10.1007/s10967-014-3228-5>.
- [21] S. Sarina, A. Bo, D. Liu, H. Liu, D. Yang, C. Zhou, N. Maes, S. Komarneni, H. Zhu, Separate or simultaneous removal of radioactive cations and anions from water by layered sodium vanadate-based sorbents, *Chem. Mater.* 26 (2014) 4788–4795, <https://doi.org/10.1021/cm501846z>.
- [22] D. McNulty, D. Noel, C.O. Dwyer, Optimizing the structure and yield of vanadium oxide nanotubes by periodic 2D layer scrolling, *RSC Adv.* 6 (2016) 40932–40944, <https://doi.org/10.1039/C6RA04853F>.
- [23] F. Krumeich, H. Muhr, M. Niederberger, F. Bieri, B. Schnyder, R. Nesper, Morphology and topochemical reactions of novel vanadium oxide nanotubes, *J. Am. Chem. Soc.* 121 (1999) 8324–8331, <https://doi.org/10.1021/ja991085a>.
- [24] J.M. Reinoso, H.-J. Muhr, F. Krumeich, F. Bieri, R. Nesper, Controlled uptake and release of metal cations by vanadium oxide nanotubes, *Helv. Chim. Acta* 83 (2000) 1724–1733, [https://doi.org/10.1002/1522-2675\(20000809\)83:8<1724::AID-HLCA1724>3.0.CO;2-G](https://doi.org/10.1002/1522-2675(20000809)83:8<1724::AID-HLCA1724>3.0.CO;2-G).
- [25] W.-N. Li, J. Yuan, S. Gomez-Mower, S. Sithambaram, S.L. Suib, Synthesis of single crystal manganese oxide octahedral molecular sieve (OMS) nanostructures with tunable tunnels and shapes, *J. Phys. Chem. B* 110 (2006) 3066–3070, <https://doi.org/10.1021/JP0553380>.
- [26] M.K. Uddin, A review on the adsorption of heavy metals by clay minerals, with special focus on the past decade, *Chem. Eng. J.* 308 (2017) 438–462, <https://doi.org/10.1016/j.cej.2016.09.029>.
- [27] M. Ghaly, F.M.S.E. El-Dars, M.M. Hegazy, R.O. Abdel Rahman, Evaluation of synthetic Birnessite utilization as a sorbent for cobalt and strontium removal from aqueous solution, *Chem. Eng. J.* 284 (2016) 1373–1385, <https://doi.org/10.1016/j.cej.2015.09.025>.
- [28] H. Faghian, M. Moayed, A. Firooz, M. Iravani, Evaluation of a new magnetic zeolite composite for removal of Cs⁺ and Sr²⁺ from aqueous solutions: Kinetic, equilibrium and thermodynamic studies, *Comptes Rendus Chim.* 17 (2014) 108–117, <https://doi.org/10.1016/j.crci.2013.02.006>.
- [29] J.S. Wahlberg, M.J. Fishman, Adsorption of Cesium on Clay Minerals - Geological Survey Bulletin 1140-A, Washington (1962).
- [30] A. Dyer, M. Pillinger, R. Harjula, S. Amin, Sorption characteristics of radionuclides on synthetic birnessite-type layered manganese oxides, *J. Mater. Chem.* 10 (2000) 1867–1874, <https://doi.org/10.1039/b002435j>.
- [31] S. Kasap, S. Piskin, H. Tel, Titanate nanotubes: preparation, characterization and

- application in adsorption of strontium ion from aqueous solution, *Radiochim. Acta* 100 (2012) 925–929, <https://doi.org/10.1524/ract.2012.1981>.
- [32] W. Wang, Z. Shao, Y. Liu, G. Wang, Removal of multi-heavy metals using biogenic manganese oxides generated by a deep-sea sedimentary bacterium - *Brachybacterium* sp. Strain Mn32, *Microbiology* 155 (2009) 1989–1996, <https://doi.org/10.1099/mic.0.024141-0>.
- [33] C.L. Lopano, P.J. Heaney, J.E. Post, Cs-exchange in birnessite: reaction mechanisms inferred from time-resolved X-ray diffraction and transmission electron microscopy, *Am. Mineral.* 94 (2009) 816–826, <https://doi.org/10.2138/am.2009.3068>.
- [34] J.-M. Oh, T.T. Biswick, J.-H. Choy, Layered nanomaterials for green materials, *J. Mater. Chem.* 19 (2009) 2553, <https://doi.org/10.1039/b819094a>.
- [35] B. Lanson, V.A. Drits, Q. Feng, A. Manceau, Structure of synthetic Na-birnessite: evidence for a triclinic one-layer unit cell, *Am. Mineral.* 87 (2002) 1662–1671, <https://doi.org/10.2138/am-2002-11-1215>.
- [36] O.O. Vir Singh, S.N.N. Tandon, O.O. Vir Singh, S.N.N. Tandon, Studies on the adsorption of cesium and strontium radionuclides on hydrated manganese oxide, *Int. J. Appl. Radiat. Isot.* 28 (1977) 701–704, [https://doi.org/10.1016/0020-708X\(77\)90088-6](https://doi.org/10.1016/0020-708X(77)90088-6).
- [37] R.M. McKenzie, The synthesis of Birnessite, cryptomelane, and some other oxides and hydroxides of manganese, *Mineral. Mag.* 38 (1971) 493–502, <https://doi.org/10.1180/minmag.1971.038.296.12>.
- [38] K. Kuma, W. Paplawsky, B. Gedulin, G. Arrhenius, Crystal structures of synthetic 7 Å and 10 Å manganates substituted by mono- and divalent cations, *Mineral. Mag.* 58 (1994) 425–447.
- [39] D.C. Golden, J.B. Dixon, C.C. Chen, Ion exchange, thermal transformations, and oxidizing properties of birnessite, *Clays Clay Miner.* 34 (1986) 511–520, <https://doi.org/10.1346/CCMN.1986.0340503>.
- [40] G. Kim, K. Sim, S. Kim, S. Komarneni, Y. Cho, Selective sorption of strontium using two different types of nanostructured manganese oxides, *J. Porous Mater.* 25 (2018) 321–328, <https://doi.org/10.1007/s10934-017-0548-1>.
- [41] B. Prelot, I. Ayed, F. Marchandeu, J. Zajac, On the real performance of cation exchange resins in wastewater treatment under conditions of cation competition: the case of heavy metal pollution, *Environ. Sci. Pollut. Res.* 21 (2014) 9334–9343, <https://doi.org/10.1007/s11356-014-2862-3>.
- [42] J.E. Post, D.R. Veblen, Crystal structure determinations of synthetic sodium, magnesium, and potassium birnessite using TEM and the Rietveld method, *Am. Mineral.* 7 (1990) 477–489.
- [43] T. Düren, K.S. Walton, R.Q. Snurr, Calculating geometric surface areas as a characterization tool for metal-organic frameworks, *J. Phys. Chem. C* 111 (2007) 15350–15356, <https://doi.org/10.1021/jp074723h>.
- [44] W.M. Rappé, A.K. Casewit, C.J. Colwell, K.S. Goddard III, W.A. Skiff, UFF, a full periodic table force field for molecular mechanics and molecular dynamics simulations, *J. Am. Chem. Soc.* 114 (1992) 10024–10035, <https://doi.org/10.1021/ja00051a040>.
- [45] M. Wu, L. Shi, T.-T. Lim, A. Veksha, F. Yu, H. Fan, J. Mi, Ordered mesoporous Zn-based supported sorbent synthesized by a new method for high-efficiency desulfurization of hot coal gas, *Chem. Eng. J.* 353 (2018) 273–287, <https://doi.org/10.1016/J.CEJ.2018.07.134>.
- [46] Y. Cao, H. Wei, Z. Xia, Advances in microwave assisted synthesis of ordered mesoporous materials, *Trans. Nonferrous Met. Soc. China* 19 (2009) s656–s664, [https://doi.org/10.1016/S1003-6326\(10\)60127-6](https://doi.org/10.1016/S1003-6326(10)60127-6).
- [47] Y. Li, J. Wang, Y. Zhang, M.N. Banis, J. Liu, D. Geng, R. Li, X. Sun, Facile controlled synthesis and growth mechanisms of flower-like and tubular MnO₂ nanostructures by microwave-assisted hydrothermal method, *J. Colloid Interface Sci.* 369 (2012) 123–128, <https://doi.org/10.1016/j.jcis.2011.12.013>.
- [48] F. Salles, J.-M. Douillard, R. Denoyel, O. Bildstein, M. Jullien, I. Beurroies, H. Van Damme, Hydration sequence of swelling clays: evolutions of specific surface area and hydration energy, *J. Colloid Interface Sci.* 333 (2009) 510–522, <https://doi.org/10.1016/J.JCIS.2009.02.018>.
- [49] M. Jullien, J. Raynal, É. Kohler, O. Bildstein, Physicochemical reactivity in clay-rich materials: tools for safety assessment, *Oil Gas Sci. Technol.* 60 (2005) 107–120, <https://doi.org/10.2516/ogst.2005007>.
- [50] E. Eren, M. Guney, B. Eren, H. Gumus, Performance of layered birnessite-type manganese oxide in the thermal-catalytic degradation of polyamide 6, *Appl. Catal. B Environ.* 132–133 (2013) 370–378, <https://doi.org/10.1016/J.APCATB.2012.12.006>.
- [51] E.R. Nightingale, Phenomenological Theory of Ion Solvation. Effective Radii of Hydrated Ions, *J. Phys. Chem.* 63 (1959) 1381–1387, <https://doi.org/10.1021/j150579a011>.
- [52] T. Wen, X. Wu, M. Liu, Z. Xing, X. Wang, A.-W. Xu, Efficient capture of strontium from aqueous solutions using graphene oxide-hydroxyapatite nanocomposites, *Dalton Trans.* 43 (2014) 7464–7472, <https://doi.org/10.1039/c3dt53591f>.
- [53] M. Galamboš, V. Paučová, J. Kuřčáková, O. Rosskopfová, P. Rajec, R. Adamcová, Cesium sorption on bentonites and montmorillonite K10, *J. Radioanal. Nucl. Chem.* 284 (2010) 55–64, <https://doi.org/10.1007/s10967-010-0480-1>.
- [54] Public health statement: strontium, agency toxic subst. Dis. Regist. (2004).
- [55] J.J. Mangano, J.D. Sherman, Elevated in vivo Strontium-90 from nuclear weapons test fallout among Cancer decedents: a case-control study of deciduous teeth, *Int. J. Heal. Serv.* 41 (2011) 137–158, <https://doi.org/10.2190/HS.41.1.j>.
- [56] M.R. Krejci, L. Finney, S. Vogt, D. Joester, Selective sequestration of strontium in desmid green algae by biogenic co-precipitation with barite, *ChemSusChem* 4 (2011) 470–473, <https://doi.org/10.1002/cssc.201000448>.
- [57] Y. Marcus, A simple empirical model describing the thermodynamics of hydration of ions of widely varying charges, sizes, and shapes, *Biophys. Chem.* 51 (1994) 111–127, [https://doi.org/10.1016/0301-4622\(94\)00051-4](https://doi.org/10.1016/0301-4622(94)00051-4).
- [58] B. Prelot, S. Lantenois, C. Chorro, M.-C. Charbonnel, J. Zajac, J.M. Douillard, Effect of nanoscale pore space confinement on cadmium adsorption from aqueous solution onto ordered mesoporous silica: a combined adsorption and flow calorimetry study, *J. Phys. Chem. C* 115 (2011) 19686–19695, <https://doi.org/10.1021/jp2015885>.
- [59] B. Prelot, S. Lantenois, M.-C.C. Charbonnel, F. Marchandeu, J.M. Douillard, J. Zajac, What are the main contributions to the total enthalpy of displacement accompanying the adsorption of some multivalent metals at the silica-electrolyte interface? *J. Colloid Interface Sci.* 396 (2013) 205–209, <https://doi.org/10.1016/j.jcis.2012.12.049>.
- [60] F. Salles, J.-M. Douillard, O. Bildstein, C. Gaudin, B. Prelot, J. Zajac, H. Van Damme, Driving force for the hydration of the swelling clays: case of montmorillonites saturated with alkaline-earth cations, *J. Colloid Interface Sci.* 395 (2013) 269–276, <https://doi.org/10.1016/j.jcis.2012.12.050>.
- [61] F. Salles, J.-M. Douillard, O. Bildstein, S. El Ghazi, B. Prelot, J. Zajac, H. Van Damme, Diffusion of interlayer cations in swelling clays as a function of water content: case of montmorillonites saturated with alkali cations, *J. Phys. Chem. C* 119 (2015) 10370–10378, <https://doi.org/10.1021/jp512986d>.